

# Grooved Dayem nanobridges as building blocks of high-performance $\text{YBa}_2\text{Cu}_3\text{O}_{7-\delta}$ SQUID magnetometers

Edoardo Trabaldo,<sup>†</sup> Christoph Pfeiffer,<sup>†</sup> Eric Andersson,<sup>†</sup> Riccardo Arpaia,<sup>†,‡</sup>  
 Alexei Kalaboukhov,<sup>†</sup> Dag Winkler,<sup>†</sup> Floriana Lombardi,<sup>†</sup> and Thilo Bauch<sup>\*,†</sup>

<sup>†</sup>*Quantum Device Physics Laboratory, Department of Microtechnology and Nanoscience,  
 Chalmers University of Technology, SE-41296 Göteborg, Sweden*

<sup>‡</sup>*Dipartimento di Fisica, Politecnico di Milano, Piazza Leonardo da Vinci 32, I-20133  
 Milano, Italy*

E-mail: thilo.bauch@chalmers.se

## Abstract

We present noise measurements performed on a  $\text{YBa}_2\text{Cu}_3\text{O}_{7-\delta}$  nanoscale weak-link-based magnetometer consisting of a Superconducting QUantum Interference Device (SQUID) galvanically coupled to a  $3.5 \times 3.5 \text{ mm}^2$  pick-up loop, reaching white flux noise levels and magnetic noise levels as low as  $6 \mu\Phi_0/\sqrt{\text{Hz}}$  and  $100 \text{ fT}/\sqrt{\text{Hz}}$  at  $T = 77 \text{ K}$ , respectively. The low noise is achieved by introducing Grooved Dayem Bridges (GDBs), a new concept of weak-link. A fabrication technique has been developed for the realization of nanoscale grooved bridges, which substitutes standard Dayem bridge weak links. The introduction of these novel key blocks reduces the parasitic inductance of the weak links and increases the differential resistance of the SQUIDs. This greatly improves the device performance, thus resulting in a reduction of the white noise.

*Keywords:* High-Tc, SQUID, magnetometer, YBCO, Grooved Dayem Bridge.

Superconducting QUantum Interference Devices (SQUIDs) are among the most sensitive magnetometers available today, making them one of the most prominent devices for various applications of superconducting materials. Since their introduction, SQUIDs have been used in several technological applications, e.g. geophysical surveys,<sup>1</sup> medical diagnostic (MCG and MEG)<sup>2-4</sup> and scanning SQUID microscopy.<sup>5</sup>

While the basic operation of SQUIDs is well established,<sup>6</sup> great effort is still invested in the improvement of their performance. In this respect, the recent technological advances in nano-fabrication enabled the realization of nanoSQUIDs with white flux noise levels well below  $1 \mu\Phi_0/\sqrt{\text{Hz}}$ ,<sup>7-14</sup> opening the way to single spin detection, a milestone of experimental physics.<sup>15,16</sup>

SQUIDs made of High critical Temperature Superconductors (HTS) have a much wider temperature range of operation (from mK to above 77 K) compared to their Low critical Temperature Superconductor (LTS) counterparts, greatly simplifying their practical applications. HTS SQUID magnetometers are promising candidates for future on-scalp magnetoencephalography systems.<sup>17-20</sup> Tremendous efforts have been devoted to achieve high quality HTS Josephson Junctions (JJs), the key ingredient of a SQUID, during the last few decades. This has proven to be challenging for cuprate HTS materials, due to the chemical instability, the small superconducting coherence length ( $\sim 2$  nm in the ab-planes) and the ceramic and granular nature of these materials. Nevertheless, different JJ fabrication techniques have been successfully developed for HTS SQUIDs so far. For example, high sensitivity HTS SQUIDs have been realized using grain boundary based JJs, by epitaxial growth of HTS films on bicrystal or step edge substrates.<sup>10,20-25</sup>

HTS nanoSQUIDs, realized with Dayem bridges, have also shown low magnetic flux noise properties, in combination with a simplified fabrication procedure.<sup>8,11,12</sup> However, the rather large parasitic inductance of Dayem bridges limits their implementation in SQUID magnetometers at 77 K.<sup>4</sup> Another approach to fabricate HTS weak links is by high energy ion irradiation (30-200 keV) of predefined wide YBCO bridges through a mask<sup>26</sup> or by direct

irradiation using a He focused ion beam (FIB).<sup>27</sup> This resulted in high quality low noise SQUID devices at 4 K and 50 K.<sup>28,29</sup> RF-SQUIDs working at 77 K and above have been realized showing a white flux noise level of  $100 - 200 \mu\Phi_0/\sqrt{\text{Hz}}$ ,<sup>30</sup> which is more than one order of magnitude higher than values obtained in state of the art dc-SQUIDs.<sup>20,22,23,25,31</sup> DC-SQUID devices operational at 77 K have been realized by oxygen ion irradiation, however no frequency dependent noise data have been reported.<sup>32</sup>

In this work we present a novel fabrication process of a HTS weak link: the nanoscale Grooved Dayem Bridge (GDB), which exhibits Josephson Junction-like behavior. Here, the layout of the bridge and the weak link inside the bridge are realized during one single lithography process on a  $\text{YBa}_2\text{Cu}_3\text{O}_{7-\delta}$  (YBCO) film grown on a single crystal substrate. Moreover, such weak links can be defined anywhere on the chip and freely oriented within the film plane. This approach has clear advantages compared to bicrystal HTS junctions, where the junctions are located at the grain boundary line, and to step edge junctions, which involve more than one lithography step<sup>33</sup> and several epitaxial thin film depositions.<sup>31</sup>

We have used YBCO GDBs as novel, alternative building nanoscale blocks in HTS SQUID magnetometers, which have been characterized via transport and noise measurements at  $T = 77$  K. In particular, these devices exhibit large voltage modulations ( $\Delta V = 30 - 50 \mu\text{V}$ ) and low values of white magnetic flux noise,  $6 \mu\Phi_0/\sqrt{\text{Hz}}$  (compared to the lowest reported flux noise  $4.5 \mu\Phi_0/\sqrt{\text{Hz}}$  at  $T = 77$  K<sup>25</sup>), and corresponding magnetic field noise,  $100 \text{ fT}/\sqrt{\text{Hz}}$ , at  $T = 77$  K. Therefore, GDB based SQUIDs combine the nanofabrication advantages and the device reproducibility, which are typical of Dayem bridges, with the performances, e.g. the magnetic sensitivity, of state-of-the-art SQUIDs based on grain boundary JJs.

A 50 nm thick film of YBCO is deposited by Pulsed Laser Deposition (PLD) onto a (001)  $\text{SrTiO}_3$  substrate with lateral dimensions of  $5 \times 5 \text{ mm}^2$ . On top of the YBCO film, a mask layer of amorphous hard carbon with thickness  $t_C = 110 \text{ nm}$  is deposited by PLD and defined by e-beam lithography (EBL). The device is finally patterned by gentle low energy (300 eV) Ar ion milling, as described in previous works.<sup>34,35</sup> The detailed ion milling parameters are

summarized in the supporting information, table S1. This fabrication procedure has been shown to result in YBCO nanowires with pristine bulk-like properties.<sup>34-37</sup> Here, in order to fabricate the Grooved Dayem Bridges, we start from this fabrication and take advantage of a reduced etching rate of the ion milling in specifically designed areas of the sample. To achieve this, the standard mask design for the Dayem bridge is modified, opening a gap along the full width, as shown in Figure 1(a).

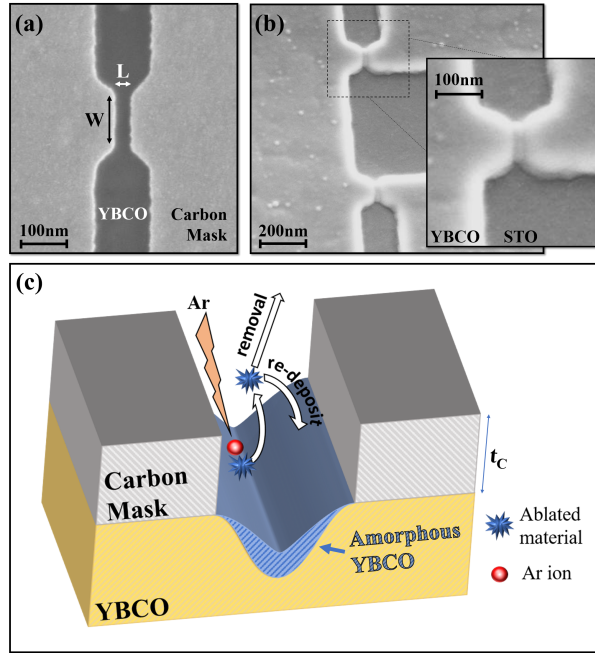


Figure 1: (a) Scanning electron microscope (SEM) image of the carbon mask on top of the YBCO film. The width and length of the gap are indicated by  $W$  and  $L$ , respectively. (b) SEM image of two GDBs after ion milling and removal of the carbon mask. The inset is the zoom-in of a single GDB. (c) Schematic of the Ar ion milling process inside the gap. The ion milled YBCO is partially redeposited as amorphous material inside the GDB gap.

The width  $W$  and length  $L$  of the gap define the geometrical dimensions of the final GDB and can be varied to achieve different values of critical current  $I_C$ . For aspect ratios of the gap in the carbon mask  $t_c/L > 2$ , the etching rate of YBCO during the Ar ion milling inside the gap is strongly reduced compared to the rest of the sample. This is the result of partial re-deposition of the YBCO ablated by the Ar ions, which cannot be removed from the gap and forms an amorphous layer of YBCO<sup>38</sup> (see Fig.1(c)). Since the etching rate inside the gap is reduced, the ion milling process required to remove 50 nm of YBCO far away from the

carbon mask edges results only in a slight thinning of the YBCO inside the gap, leaving a grooved bridge with thickness less than 50 nm. The final result obtained for a SQUID after the final ion milling is shown in Figure 1(b).

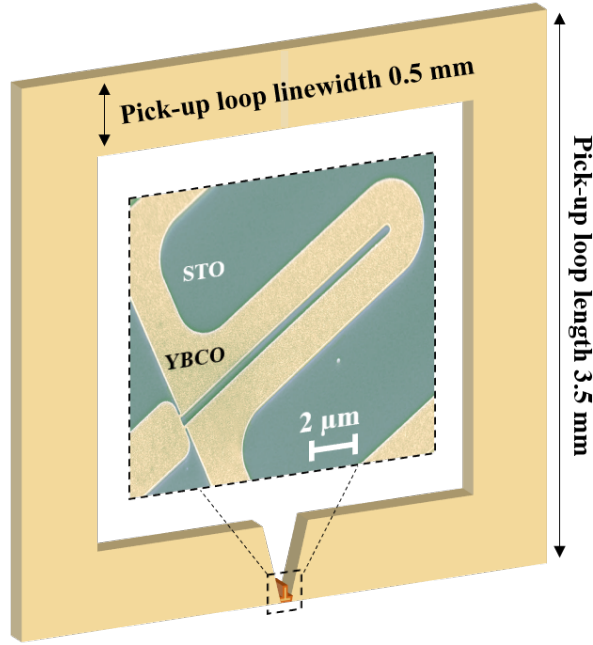


Figure 2: Schematic of the pick-up loop, with the dimensions used for the device SQ1. The inset is an SEM image, showing the details of the SQUID loop of the device SQ2, with hole dimensions  $12 \times 0.5 \mu\text{m}^2$ . The line width of the hairpin loop is  $2 \mu\text{m}$ .

Up to 16 GDB-SQUIDs can be fabricated on the same pick-up loop. The widths of the GDBs are 150 – 200 nm and the gap length in the bridge mask 50 nm. All the SQUIDs are galvanically connected to the same in plane square shaped pick-up loop of lateral dimension  $3.5 \times 3.5 \text{ mm}^2$  in order to increase the effective magnetic area  $A_{\text{eff}} = \Phi/B_a$ , with  $\Phi$  the magnetic flux through the SQUID loop and  $B_a$  the externally applied magnetic field.<sup>4,11</sup> A schematic of the pick-up loop, with only a single SQUID coupled to it, is shown in Figure 2.

When an external magnetic field  $B_a$  is applied, a screening current  $I_S \propto B_a$  circulates in the pick-up loop.  $I_S$  generates a phase difference  $\Delta\phi$  between the two weak links, which is proportional to  $I_S \cdot L_c \cdot 2\pi/\Phi_0$ , where  $\Phi_0$  is the superconducting flux quantum. Here  $L_c$  is the coupling inductance shared between the pick-up loop and the SQUID loop, i.e. the hairpin loop shown in the inset of Fig. 2. For the resulting effective area of the SQUID

$A_{eff} = \Phi_0/2\pi \cdot \Delta\phi/B_a$  one can write<sup>11</sup>

$$A_{\text{eff}} = A_{\text{nS}} + A_{\text{eff}}^{\text{pl}} \frac{L_c}{L_{\text{loop}}}, \quad (1)$$

where  $A_{\text{nS}}$  is the effective area of the SQUID loop,  $A_{\text{eff}}^{\text{pl}}$  is the effective area of the pick-up loop and  $L_{\text{loop}}$  is the inductance of the pick-up loop. A more detailed analysis of the effect of a pick-up loop on the SQUID performance can be found in Refs.<sup>4,11</sup>  $L_c$  has been measured in a separate experiment by direct current injection and it is directly proportional to the length of the hairpin slit  $l_{\text{slit}}$ . It can be approximated from the measured data as  $L_c \simeq l_{\text{slit}} \cdot 8 \text{ pH}/\mu\text{m}$  at  $T = 77 \text{ K}$  and is mainly dominated by kinetic inductance  $L_k \simeq 2l_{\text{slit}}\mu_0\lambda_L^2/w_{\text{hl}}t$ , with  $\mu_0$  the vacuum permeability,  $w_{\text{hl}} = 2 \mu\text{m}$  the line width of the hair pin loop,  $t$  the thickness of the YBCO film, and  $\lambda_L \simeq 565 \text{ nm}$  the in plane London penetration depth at 77 K.<sup>11</sup>

Table 1: Summary of the SQUIDs geometrical and transport parameters at  $T = 77 \text{ K}$ .

Name	Coupling	$l_{\text{slit}}$ [ $\mu\text{m}$ ]	$W$ [nm]	$L$ [nm]	$I_C$ [ $\mu\text{A}$ ]	$\Delta V$ [ $\mu\text{V}$ ]	$L_C$ [pH]	$A_{\text{eff}}$ [ $\text{mm}^2$ ]	$I_C\delta R$ [ $\mu\text{V}$ ]	$I_C R_N$ [ $\mu\text{V}$ ]
SQ1	Pick-up loop	20	200	50	15	30	160	0.122	187	346
SQ2	Direct current injection	12	150	50	7	50	96	-	168	364

The GDB-SQUIDs have been characterized via electrical transport and noise measurements, performed in a magnetically shielded room (shielding factor  $10^2 - 10^5$  in the frequency range 0.1 Hz–1 kHz) at liquid nitrogen temperature,  $T \simeq 77 \text{ K}$ . A summary of the geometric dimensions and electric transport properties of two SQUIDs patterned on two different chips are reported in Table 1. SQ2 didn't have a pick-up loop but was measured with direct current injection. Here, a modulation current  $I_m$  is applied directly to the SQUID loop, which acts as an effective magnetic flux  $I_m \times L_c$ , therefore inducing modulations of critical current  $I_C$ .<sup>39</sup>

The two current voltage characteristics (IVCs) shown in Figure 3(a) for SQ1 correspond to the maximum,  $I_C^{\text{max}}$ , and the minimum,  $I_C^{\text{min}}$ , measured values of the positive critical

current within one modulation period. Figure 3(b) shows the modulation of the critical current,  $I_C(\Phi)$ , where  $\Phi$  is the applied magnetic flux. Similarly to what has been shown in our previous works on Dayem bridge SQUIDs,<sup>8,11,12</sup> our GDB based SQUIDs exhibit modulations of the critical current  $I_C$  as a function of the externally applied magnetic flux. The IVCs and  $I_C$  modulation for SQ2 are reported in the supporting information showing similar behavior as SQ1.

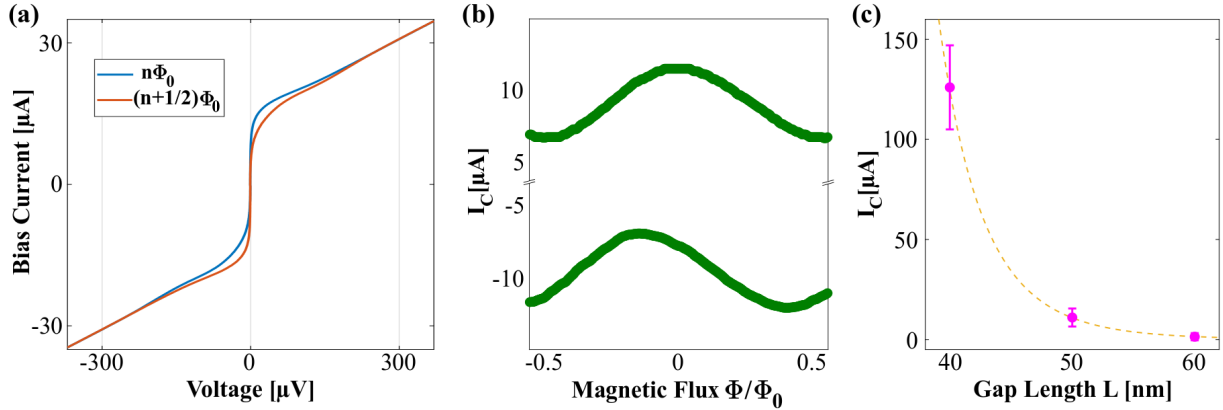


Figure 3: (a) Current Voltage Characteristics (IVCs) of SQUID SQ1 at 77 K. The red and blue curves correspond respectively to the maximum and to the minimum value of the positive critical current  $I_C$  within one modulation period. The asymmetry in the modulation between positive and negative bias currents is a consequence of the used asymmetric biasing scheme. (b) Modulation of  $I_C$  as a function of the applied magnetic flux. (c) Average  $I_C$  measured on several GDBs for various gap lengths  $L$  and fixed bridge width  $W = 200$  nm. The error bars are obtained as the standard deviations of the  $I_C$  measured on an ensemble of devices. Over 9 different fabricated chips the total amount of measured devices are 28, 56 and 16 for  $L = 40, 50$  and  $60$  nm respectively. The dashed line is a guide for the eye.

The shape of the IVC resembles that of a resistively shunted junction (RSJ) similar to junctions defined with a focused helium ion beam,<sup>27</sup> indicative of a superconductor-normal conductor-superconductor (SNS) type of junction at 77 K. The RSJ-like behavior persists down to  $T = 4.2$  K (see supporting information), a feature not observed in ,e.g., oxygen irradiated bridges.<sup>32</sup> Here it is important to point out that the characteristic voltage of GDBs  $I_C R_N \simeq 350 \mu\text{V}$ , with  $R_N$  the differential resistance taken in the voltage range  $V = 300 - 500 \mu\text{V}$ , is at least a factor of 10 larger than He ion irradiated junctions reported in literature at 77 K.<sup>27</sup> The highest  $I_C R_N$  products at liquid nitrogen temperature have been achieved

with grain boundary junctions,<sup>40,41</sup> with characteristic voltages in the range 800 – 1200  $\mu\text{V}$ . Bicrystal and step-edge JJs are generally believed to be closer to tunnel-like superconductor-insulator-superconductor (SIS) JJs and they are expected to have higher  $I_C R_N$  products compared to SNS-type JJs. While the characteristic voltages of GDBs presented here are lower than for grain boundary junctions, GDB-based SQUID magnetometers are in the same performance range as those realized by state-of-the-art junction technologies as will be shown below. A more in depth analysis on the properties of GDBs is beyond the scope of this letter and will be reported elsewhere.

The reproducibility of the fabrication process introduced above is supported by the small spread of the measured  $I_C$  values at  $T = 77$  K of Grooved Dayem Bridges patterned on different chips, see Fig. 3(c). Here the gap length  $L$  is varied between 40 and 60 nm and the bridge width is kept fixed  $W = 200$  nm. For  $L = 40$  nm, the average  $I_C$  is  $130 \pm 20 \mu\text{A}$  and for  $L = 50$  nm we measured an average  $I_C$  of  $10 \pm 4 \mu\text{A}$ . When  $L$  is increased to 60 nm,  $I_C$  is suppressed to a few  $\mu\text{A}$  or in most cases no supercurrent could be detected. After several cooling cycles and more than 3 months storage at room temperature, the values of  $I_C$  do not significant deviate from the original results.

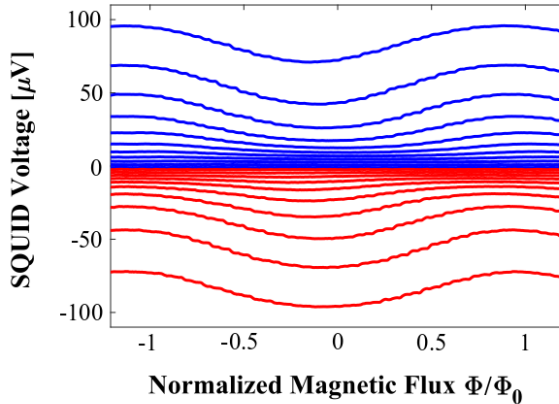


Figure 4: Voltage modulations of SQUID SQ1 as a function of the magnetic flux for increasing values of the bias current.

In the following we discuss the advantages of using GDB-based SQUIDS compared to



those implementing Dayem bridges: 1) the critical current density of  $2.5 \cdot 10^5$  A/cm<sup>2</sup> is 40 times smaller than those of Dayem bridges. This allows implementing wider GDB junctions in SQUID magnetometers resulting in a smaller parasitic inductance, which scales with  $\lambda_L^2/Wt$ . Hence a larger coupling inductance (hair pin loop) can be used for increasing the effective area<sup>4</sup> while keeping the screening parameter near the optimal value  $\beta_L = I_C \cdot L_{\text{sq}}/\Phi_0 \simeq 1$ , where  $L_{\text{sq}}$  is the total SQUID loop inductance; 2) the resistivity of GDBs is approximately  $0.15 \text{ } \Omega\mu\text{m}^2$ , which is roughly 50 times larger than those of Dayem bridges. The larger resistivity of GDB results in an increased voltage modulation depth, reducing the contribution of the readout electronics input noise to the total flux noise, which will be discussed in the following.

The SQUID noise has been measured using a commercial Magnicon SEL-1 dc SQUID electronics.<sup>42</sup> The system allows to perform measurements in Flux Locked Loop (FLL) mode and use current bias reversal at 40 kHz in order to reduce the low-frequency critical current noise.<sup>43</sup>

The measured voltage modulations of SQ1 as a function of magnetic flux are shown in Figure 4 for various bias current values. Each curve corresponds to an increment of the bias current equal to  $1.8 \text{ } \mu\text{A}$ . We obtain a voltage modulation depth  $\Delta V \simeq 30 \text{ } \mu\text{V}$  for values of the bias current slightly above  $I_C$ . For the transfer function  $V_\Phi$  defined as  $\max(\delta V/\delta\Phi) \simeq \pi\Delta V/\Phi_0$ , corresponding to the maximum voltage response of the SQUID per unit of flux, we obtain  $V_\Phi = 115 \text{ } \mu\text{V}/\Phi_0$ . Indeed, a large voltage modulation depth  $\Delta V \simeq \delta R \Delta I_C$ , with  $\Delta I_C$  the critical current modulation depth and  $\delta R$  the differential resistance of the SQUID at the working point (see supporting information) is required to achieve low noise SQUID devices. By doing so, the contribution of the amplifier input voltage noise  $S_{V,a}^{1/2}$  to the white flux noise  $S_{\Phi,a}^{1/2} \simeq \Phi_0 S_{V,a}^{1/2}/\pi\Delta V$  of the SQUID is minimized, hence improving the device performance.

The effective area  $A_{\text{eff}}$  was determined via responsivity measurements, i.e. measuring the SQUID response in FLL mode to a known magnetic field. The value of the effective area

for SQ1, which is galvanically coupled to a pick-up loop with dimensions  $3.5 \times 3.5 \text{ mm}^2$ , is  $A_{\text{eff}} = 0.122 \text{ mm}^2$ . This value is consistent with previously reported measurements performed on similar devices implementing YBCO Dayem bridges.<sup>4</sup> The voltage noise  $S_V^{1/2}$  for SQUID SQ1 was measured in FLL mode using current bias reversal. The resulting magnetic flux noise  $S_\Phi^{1/2} = S_V^{1/2}/V_\Phi$  and magnetic field noise  $S_B^{1/2} = S_\Phi^{1/2}/A_{\text{eff}}$  are shown in Figure 5.

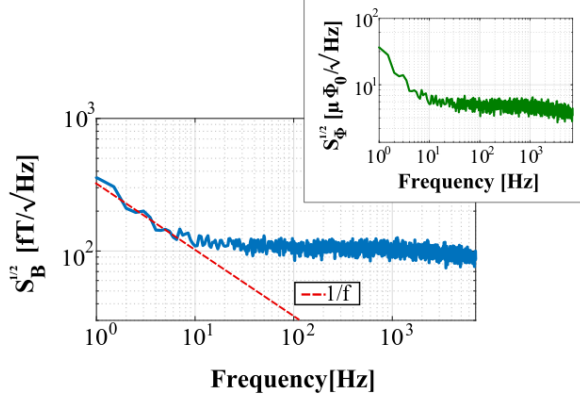


Figure 5: Magnetic field noise  $S_B$  measured on SQ1 with bias reversal scheme. The red line indicates the  $1/f$  noise. Inset: magnetic flux noise  $S_\Phi$ .

We observe a white flux noise level  $S_\Phi^{1/2} \simeq 6 \mu\Phi_0/\sqrt{\text{Hz}}$  above the  $1/f$  knee frequency of  $f \simeq 10 \text{ Hz}$  (see inset of Figure 5). This noise value is close to the expected readout electronics input noise,  $4 \mu\Phi_0/\sqrt{\text{Hz}}$ . The corresponding white magnetic noise is  $S_B^{1/2} \simeq 100 \text{ fT}/\sqrt{\text{Hz}}$  (see Figure 5). This is a high level of sensitivity for a device with a much smaller pick-up loop ( $3.5 \times 3.5 \text{ mm}^2$ ) than standard magnetometers ( $8 \times 8 \text{ mm}^2$  and above<sup>4,40</sup>). Comparing these values to Dayem bridge based magnetometers<sup>4</sup> GDB-based devices have 10 times lower flux and magnetic field noise. This is even more remarkable considering the much smaller pick-up loop size used in this work compared to the one used in Ref.<sup>4</sup>

The achieved white magnetic flux noise values are comparable to state of the art single layer grain boundary junction based YBCO SQUIDS,  $S_\Phi^{1/2} = 4.5 - 10 \mu\Phi_0/\sqrt{\text{Hz}}$ .<sup>20,22,23,25,31</sup> Single layer grain boundary based SQUIDS galvanically coupled to a pick-up loop of  $\sim 8 \times 8 \text{ mm}^2$  have reached white magnetic field noise values down to  $S_B^{1/2} = 30 - 50 \text{ fT}/\sqrt{\text{Hz}}$ .<sup>20,23,31</sup> These values are a factor 2–3 lower than the one shown in Figure 5. However, considering the

small size of the used pick-up loop,  $3.5 \times 3.5 \text{ mm}^2$ , implemented in this work, grooved Dayem bridge based magnetometers should reach similar or even better magnetic field sensitivities for pick-up loops of lateral dimension  $8 - 10 \text{ mm}$ . The effective area of a magnetometer, and hence the magnetic field noise, can be further improved by implementing a superconducting flux transformer in a flip-chip setup.<sup>40</sup> Values below  $10 \text{ fT}/\sqrt{\text{Hz}}$  have been achieved in grain boundary JJ based devices.<sup>40</sup> Implementing a flux transformer in our GDB based SQUID devices would indeed further improve the magnetic field sensitivity.

In conclusion, we have developed a reproducible nanopatterning procedure for the realization of YBCO Grooved Dayem Bridges. Here the layout of the bridge and the weak link across it are realized during one single lithography process on a YBCO film grown on a single crystal substrate. Such weak links have been implemented in SQUIDs galvanically coupled to a square shaped in-plane pick-up loop with lateral dimension of  $3.5 \text{ mm}$ . The smaller critical current densities and larger differential resistances of the GDBs compared to bare Dayem bridges allows to implement wider bridges in SQUID application and therefore reducing the parasitic inductance. We obtained a voltage modulation depth  $\Delta V \simeq 30 \mu\text{V}$  for a SQUID with hair pin slit length  $l_{\text{slit}} = 20 \mu\text{m}$  and an effective area  $A_{\text{eff}} = 0.122 \text{ mm}^2$ .

The achieved magnetic field noise of  $100 \text{ fT}/\sqrt{\text{Hz}}$  on such a small device ( $3.5 \times 3.5 \text{ mm}^2$ ) paves the ground for the realization of a single layer YBCO magnetometer with magnetic field noise below  $25 \text{ fT}/\sqrt{\text{Hz}}$ . This could be achieved on a  $10 \times 10 \text{ mm}^2$  substrate and using a slightly longer hair pin SQUID loop. This work proves the feasibility of Grooved Dayem Bridges for the fabrication of high quality weak links and for SQUID applications. The development of low noise HTS SQUIDs is crucial not only for technological applications, such as medical diagnostic (MCG and MEG)<sup>2-4</sup> and geophysical surveys,<sup>1</sup> but also in fundamental research, e.g. for magnetization measurements of nanoscale particles and single spin detection.<sup>10</sup> Moreover, GDBs could open the way to a range of future applications, such as HTS rapid single flux quantum (RSFQ) circuits<sup>44</sup> and high-performance high-frequency HTS superconducting quantum interference filters (SQIFs).<sup>45</sup>

## Acknowledgement

The authors acknowledge helpful discussions with T. Claeson and D. Montemurro. This work was been supported in part by the Knut and Alice Wallenberg Foundation (KAW) and in part by the Swedish Research Council (VR). R. A. is supported by the Swedish Research Council (VR) under the project "Evolution of nanoscale charge order in superconducting YBCO nanostructures".

## Supporting Information Available

The following files are available free of charge.

The following files are available.

- Supporting Information: Ion milling parameters summary, current voltage characteristic for SQ2, differential resistance and modulation depth as a function of bias current for both SQ1 and SQ2.

## References

- (1) Clarke, J. Geophysical applications of SQUIDS. *IEEE Trans. Magn.* **1983**, *19*, 288–294.
- (2) Koch, H. SQUID magnetocardiography: Status and perspectives. *IEEE Trans. Appl. Supercond.* **2001**, *11*, 49–59.
- (3) Öisjöen, F.; Schneiderman, J. F.; Astalan, A. P.; Kalabukhov, A.; Johansson, C.; Winkler, D. A new approach for bioassays based on frequency-and time-domain measurements of magnetic nanoparticles. *Biosens. Bioelectron* **2010**, *25*, 1008–1013.
- (4) Xie, M.; Chukharkin, M.; Ruffieux, S.; Schneiderman, J.; Kalabukhov, A.; Arzeo, M.; Bauch, T.; Lombardi, F.; Winkler, D. Improved coupling of nanowire-based high-T c

- SQUID magnetometers – Simulations and experiments. *Supercond. Sci. Tech.* **2017**, *30*, 115014.
- (5) Vasyukov, D.; Anahory, Y.; Embon, L.; Halbertal, D.; Cuppens, J.; Neeman, L.; Finkler, A.; Segev, Y.; Myasoedov, Y.; Rappaport, M. L. a. A scanning superconducting quantum interference device with single electron spin sensitivity. *Nat. Nanotechnol.* **2013**, *8*, 639.
- (6) Clarke, J.; Braginski, A. I. *The SQUID handbook: Applications of SQUIDs and SQUID systems*; John Wiley & Sons, 2006.
- (7) Granata, C.; Vettoliere, A.; Russo, R.; Fretto, M.; De Leo, N.; Lacquaniti, V. Three-dimensional spin nanosensor based on reliable tunnel Josephson nano-junctions for nanomagnetism investigations. *Appl. Phys. Lett.* **2013**, *103*, 102602.
- (8) Arpaia, R.; Arzeo, M.; Nawaz, S.; Charpentier, S.; Lombardi, F.; Bauch, T. Ultra low noise YBa<sub>2</sub>Cu<sub>3</sub>O<sub>7- $\delta$</sub>  nano superconducting quantum interference devices implementing nanowires. *Appl. Phys. Lett.* **2014**, *104*, 072603.
- (9) Wölbing, R.; Schwarz, T.; Müller, B.; Nagel, J.; Kemmler, M.; Kleiner, R.; Koelle, D. Optimizing the spin sensitivity of grain boundary junction nanoSQUIDs – towards detection of small spin systems with single-spin resolution. *Supercond. Sci. Technol.* **2014**, *27*, 125007.
- (10) Schwarz, T.; Wölbing, R.; Reiche, C. F.; Müller, B.; Martínez-Pérez, M.-J.; Mühl, T.; Büchner, B.; Kleiner, R.; Koelle, D. Low-noise YBa<sub>2</sub>Cu<sub>3</sub>O<sub>7</sub> nano-SQUIDs for performing magnetization-reversal measurements on magnetic nanoparticles. *Phys. Rev. Appl.* **2015**, *3*, 044011.
- (11) Arzeo, M.; Arpaia, R.; Baghdadi, R.; Lombardi, F.; Bauch, T. Toward ultra high magnetic field sensitivity YBa<sub>2</sub>Cu<sub>3</sub>O<sub>7- $\delta$</sub>  nanowire based superconducting quantum interference devices. *J. Appl. Phys.* **2016**, *119*, 174501.

- (12) Arpaia, R.; Arzeo, M.; Baghdadi, R.; Trabaldo, E.; Lombardi, F.; Bauch, T. Improved noise performance of ultrathin YBCO Dayem bridge nanoSQUIDs. *Supercond. Sci. Technol.* **2016**, *30*, 014008.
- (13) Chen, L.; Wang, H.; Liu, X.; Wu, L.; Wang, Z. A High-performance Nb nano-superconducting quantum interference device with a three-dimensional structure. *Nano Lett.* **2016**, *16*, 7726–7730.
- (14) Russo, R.; Esposito, E.; Crescitelli, A.; Di Gennaro, E.; Granata, C.; Vettoliere, A.; Cristiano, R.; Lisitskiy, M. NanoSQUIDs based on niobium nitride films. *Supercond. Sci. Technol.* **2016**, *30*, 024009.
- (15) Martínez-Pérez, M. J.; Koelle, D. NanoSQUIDs: Basics & recent advances. *Phys. Sci. Rev.* **2016**, *2*.
- (16) Granata, C.; Vettoliere, A. Nano superconducting quantum interference device: A powerful tool for nanoscale investigations. *Phys. Rep.* **2016**, *614*, 1–69.
- (17) Schneiderman, J. F. Information content with low-vs. high-T<sub>c</sub> SQUID arrays in MEG recordings: The case for high-T<sub>c</sub> SQUID-based MEG. *J. Neurosci. Methods* **2014**, *222*, 42–46.
- (18) Xie, M.; Schneiderman, J. F.; Chukharkin, M. L.; Kalabukhov, A.; Riaz, B.; Lundqvist, D.; Whitmarsh, S.; Hämäläinen, M.; Jousmäki, V.; Oostenveld, R.; Winkler, D. Benchmarking for on-scalp MEG sensors. *IEEE Trans. Biomed. Eng.* **2017**, *64*, 1270–1276.
- (19) Riaz, B.; Pfeiffer, C.; Schneiderman, J. F. Evaluation of realistic layouts for next generation on-scalp MEG: spatial information density maps. *Sci. Rep.* **2017**, *7*, 6974.
- (20) Öisjöen, F.; Schneiderman, J. F.; Figueras, G.; Chukharkin, M.; Kalabukhov, A.; Hedström, A.; Elam, M.; Winkler, D. High-T<sub>c</sub> superconducting quantum interference

- device recordings of spontaneous brain activity: Towards high-T<sub>c</sub> magnetoencephalography. *Appl. Phys. Lett.* **2012**, *100*, 132601.
- (21) Lee, L.; Teepe, M.; Vinetskiy, V.; Cantor, R.; Colclough, M. Key elements for a sensitive 77 K direct current superconducting quantum interference device magnetometer. *Applied physics letters* **1995**, *66*, 3058–3060.
- (22) Faley, M.; Poppe, U.; Dunin-Borkowski, R.; Schiek, M.; Boers, F.; Chocholacs, H.; Dammers, J.; Eich, E.; Shah, N.; Ermakov, A. High-T<sub>c</sub> DC SQUIDS for magnetoencephalography. *IEEE Trans. Appl. Supercond.* **2013**, *23*, 1600705–1600705.
- (23) Chukharkin, M.; Kalabukhov, A.; Schneiderman, J. F.; Öisjöen, F.; Jönsson, M.; Xie, M.; Snigirev, O. V.; Winkler, D. Improvement of ultra-low field magnetic resonance recordings with a multilayer flux-transformer-based high-T<sub>c</sub> SQUID magnetometer. *IEEE Trans. Appl. Supercond.* **2013**, *23*.
- (24) Chesca, B.; John, D.; Mellor, C. J. Flux-coherent series SQUID array magnetometers operating above 77 K with superior white flux noise than single-SQUIDS at 4.2 K. *Applied Physics Letters* **2015**, *107*, 162602.
- (25) Mitchell, E.; Foley, C. YBCO step-edge junctions with high I<sub>c</sub>R<sub>n</sub>. *Supercond. Sci. Technol.* **2010**, *23*, 065007.
- (26) Tinchev, S. S. Mechanism of operation of josephson junctions made from htc materials by ion modification. *Physica C: Superconductivity* **2007**, *460*, 1477–1478.
- (27) Cybart, S. A.; Cho, E.; Wong, T.; Wehlin, B. H.; Ma, M. K.; Huynh, C.; Dynes, R. Nano Josephson superconducting tunnel junctions in YBa<sub>2</sub>Cu<sub>3</sub>O<sub>7-δ</sub> directly patterned with a focused helium ion beam. *Nat. Nanotech.* **2015**, *10*, 598.
- (28) Cho, E.; Ma, M.; Huynh, C.; Pratt, K.; Paulson, D.; Glyantsev, V.; Dynes, R.; Cybart, S. A. YBa<sub>2</sub>Cu<sub>3</sub>O<sub>7-δ</sub> superconducting quantum interference devices with metallic

- to insulating barriers written with a focused helium ion beam. *Appl. Phys. Lett.* **2015**, *106*, 252601.
- (29) Cho, E. Y.; Li, H.; LeFebvre, J. C.; Zhou, Y. W.; Dynes, R.; Cybart, S. A. Direct-coupled micro-magnetometer with Y-Ba-Cu-O nano-slit SQUID fabricated with a focused helium ion beam. *Applied physics letters* **2018**, *113*, 162602.
- (30) Tinchev, S. High-T/sub c/SQUIDS with local oxygen-ion irradiated weak links. *IEEE transactions on applied superconductivity* **1993**, *3*, 28–32.
- (31) Faley, M.; Meertens, D.; Poppe, U.; Dunin-Borkowski, R. Graphoepitaxial high-Tc SQUIDs. *Journal of Physics: Conference Series*. 2014; p 042009.
- (32) Bergeal, N.; Lesueur, J.; Faini, G.; Aprili, M.; Contour, J. High T c superconducting quantum interference devices made by ion irradiation. *Applied physics letters* **2006**, *89*, 112515.
- (33) Foley, C. Fabrication and characterisation of YBCO single grain boundary step edge junctions. *IEEE Trans. Appl. Supercond.* **1999**, *9*, 4281–4284.
- (34) Nawaz, S.; Arpaia, R.; Lombardi, F.; Bauch, T. Microwave Response of Superconducting Y Ba 2 Cu 3 O 7-  $\delta$  Nanowire Bridges Sustaining the Critical Depairing Current: Evidence of Josephson-like Behavior. *Phys. Rev. Lett.* **2013**, *110*, 167004.
- (35) Nawaz, S.; Arpaia, R.; Bauch, T.; Lombardi, F. Approaching the theoretical depairing current in YBa<sub>2</sub>Cu<sub>3</sub>O<sub>7-x</sub> nanowires. *Physica C Supercond* **2013**, *495*, 33–38.
- (36) Trbaldo, E.; Arzeo, M.; Arpaia, R.; Baghdadi, R.; Andersson, E.; Lombardi, F.; Bauch, T. Noise properties of YBCO Nanostructures. *IEEE Trans. Appl. Supercond.* **2017**, *27*.
- (37) Arpaia, R.; Andersson, E.; Trbaldo, E.; Bauch, T.; Lombardi, F. Probing the phase



- diagram of cuprates with  $\text{YBa}_2\text{Cu}_3\text{O}_{7-\delta}$  thin films and nanowires. *Phys. Rev. Mater.* **2018**, *2*, 024804.
- (38) Manos, D. M.; Flamm, D. L. *Plasma etching: an introduction*; Elsevier, 1989.
- (39) Johansson, J.; Cedergren, K.; Bauch, T.; Lombardi, F. Properties of inductance and magnetic penetration depth in (103)-oriented  $\text{YBa}_2\text{Cu}_3\text{O}_{7-\delta}$  thin films. *Phys. Rev. B* **2009**, *79*, 214513.
- (40) Faley, M.; Dammers, J.; Maslennikov, Y.; Schneiderman, J.; Winkler, D.; Koshelets, V.; Shah, N.; Dunin-Borkowski, R. High-Tc SQUID biomagnetometers. *Superconductor Science and Technology* **2017**, *30*, 083001.
- (41) Poppe, U.; Divin, Y.; Faley, M.; Wu, J.; Jia, C.; Shadrin, P.; Urban, K. Properties of  $\text{YBa}_2\text{Cu}_3\text{O}_7$  thin films deposited on substrates and bicrystals with vicinal offcut and realization of high  $I_c/R_n$  junctions. *IEEE transactions on applied superconductivity* **2001**, *11*, 3768–3771.
- (42) Magnicon, *SQUID electronics SEL-1*, <http://www.magnicon.com>.
- (43) Drung, D. High-Tc and low-Tc dc SQUID electronics. *Supercond. Sci. Technol.* **2003**, *16*, 1320.
- (44) Wolf, T.; Bergeal, N.; Lesueur, J.; Fourie, C. J.; Faini, G.; Ulysse, C.; Fevbre, P. YBCO Josephson junctions and striplines for RSFQ circuits made by ion irradiation. *IEEE Transactions on applied superconductivity* **2013**, *23*, 1101205–1101205.
- (45) Mitchell, E.; Hannam, K.; Lazar, J.; Leslie, K.; Lewis, C.; Grancea, A.; Keenan, S.; Lam, S.; Foley, C. 2D SQIF arrays using 20 000 YBCO high  $R_n$  Josephson junctions. *Supercond. Sci. Technol.* **2016**, *29*, 06LT01.